Ferrimagnetism and spin reorientation in the high-pressure double double perovskites CaMnCrSbO6 and CaMnFeSbO6

Ferrimagnetism and spin reorientation in the high pressure double double perovskites $CaMnCrSbO_6$ and $CaMnFeSbO_6$

Elena Solana-Madruga[1*], Padraig S. Kearins[1], Khalid N. Alharbi[1], Ciaran T. Lennon[1], Clemens Ritter[2] and J. Paul Attfield[1]

[1] Centre for Science at Extreme Conditions (CSEC) and School of Chemistry, University of Edinburgh, EH9 3FD, U.K.
[2] Institut Laue-Langevin, 38042 Grenoble Cedex, France.
(Received xxxx)

Two new $CaMnBSbO_6$ (B = Cr and Fe) high pressure double double perovskites are reported. Spins in $CaMnCrSbO_6$ order below T_C = 49 K into a collinear ferrimagnetic arrangement with spins in the xy plane. $CaMnFeSbO_6$ has the same ordered magnetic structure below T_{C1} = 55 K, but also shows a second magnetic transition at T_{C2} = 21 K where the spins reorient towards the z axis. This may reflect a greater degree of magnetic disorder for B = Fe and A-B intersite charge transfer may also be significant.

I. INTRODUCTION

Compounds of general formula ABO_3 with the perovskite structure accept a wide range of A and B site cations, and can give rise to $AA'B_2O_6$ or $A_2BB'O_6$ double perovskites.[1] However, the combination of cation order into both sublattices is uncommon. Among the nine possible double double (doubly ordered) $AA'BB'O_6$ structures,[2] only those combining rock-salt order of B-site cations with layered[3,4] or columnar A cation order have been reported. The latter type was recently reported for $MnRMnSbO_6$ (R = rare earth)[5,6] and $CaMnBReO_6$ (B = transition metal)[7,8] compositions. Both systems show a rich variety of magnetic properties. The rare earth materials show multiple magnetic transitions and have strong magnetic anisotropy[6]. $CaMnFeReO_6$ has robust Fe^{3+}/Re^{5+} ferrimagnetic order at ~ 500 K and exhibits negative magnetoresistance at low temperatures.[7] $CaMnB^{2+}Re^{6+}O_6$ are ferrimagnetic for $B = Co^{2+}$, ferromagnetic for $B = Ni^{2+}$ [8] and two perpendicular spin sublattices for A and B site cations are reported for antiferomagnetic $B = Mn^{2+}$.[7]

A recent study of compositions between Ca_2FeReO_6 [9,10] and Mn_2FeReO_6[11,12] revealed little miscibility between the double perovskite end members and the double double perovskite $CaMnFeReO_6$ formed at the midpoint of the series.[13] However, a coherent evolution of magnetic properties with high-T_C Fe-Re spin order and low temperature magnetic order of Mn^{2+} spins was observed throughout. The Ca_2BSbO_6 and Mn_2BSbO_6 (B = Cr, Fe) double perovskites, however, show different magnetic behaviors, with strong frustration in the Ca-based materials leading to low temperaure ferromagnetism (B = Cr) and spin-glass behaviour (B = Fe),[14,15] while the high pressure Mn-analogs show antiferromagnetism with a helical spin order for B = Fe) below 60 K.[16,17] We have thus investigated the double double perovskites formed between these two pairs and we report here the structures and magnetic properties of the two new high pressure double double perovskite oxides $CaMnBSbO_6$ (B = Cr and Fe).

II. EXPERIMENTAL

Polycrystalline $CaMnBSbO_6$ samples were synthesized under high pressure and high temperature conditions. The precursors were prepared by mixing stoichiometric proportions of $CaMnO_3$, Cr_2O_3 and Sb_2O_3 for $CaMnCrSbO_6$, and $Ca_2Fe_2O_5$, MnO and Sb_2O_5 for $CaMnFeSbO_6$. $CaMnO_3$ was prepared by heating stoichiometric amounts of $CaCO_3$ and MnO at 1200 ºC under a N_2 flow in increasing temperature steps, and $Ca_2Fe_2O_5$ was made by heating $CaCO_3$ and Fe_2O_3 at 1200 ºC. The precursor mixtures were packed into Pt capsules and compressed to 10 GPa using a Walker-type multianvil press. Samples were heated at 1100 ºC for 20 minutes and quenched, after which pressure was slowly released.

Powder X-ray diffraction was used to confirm that double double perovskites were formed in both samples. Neutron Powder Diffraction (NPD) data were collected for ~50 mg samples using the D20 beamline at the Institut Laue-Langevin (Grenoble, France). The $0 < 2\theta < 130$º angular range was covered with a 0.1º step size. Long scans were taken at 1.5, 65 and 300 K for $CaMnCrSbO_6$ using wavelength λ = 1.87 Å and at 3, 35 and 70 K for $CaMnFeSbO_6$ using λ = 2.41 Å for refinement of their nuclear and

magnetic structures. A scan in high resolution mode was also collected at 300 K for $CaMnFeSbO_6$ using λ = 1.54 Å. Additional short scans were collected from 5 to 65 K every 1.2 K for $CaMnFeSbO_6$ to study the thermal evolution of magnetic structure through the two discovered magnetic transitions. The magnetic symmetry analysis was performed using BasIreps [18] and the diffraction patterns were fitted through the Rietveld method using the Fullprof package. [19] Magnetization measurements were made using a MPMS Quantum Design magnetometer. Temperature dependence of the magnetization was scanned in field cooled (FC) and zero field cooled (ZFC) modes.

III. RESULTS AND DISCUSSION

A. Crystal Structures

Fits to 300 K NPD data (Fig. 1) confirm that $CaMnCrSbO_6$ and $CaMnFeSbO_6$ adopt double double perovskite structures in space group $P4_2/n$. The relative values of cell parameters are consistent with the larger ionic radius of Fe^{3+} (0.745 Å) compared to Cr^{3+} (0.715 Å)[20]. The neutron scattering lengths of Ca, Mn, Cr/Fe and Sb (4.70, -3.73, 3.64/9.45 and 5.57 fm respectively) provide good contrast cation site allowing precise occupancies to be refined. The Ca site was found to be fully occupied but cation mixing was observed at all other sites, as shown in Table I. Partial *B* occupation is observed at both the tetrahedral Mn' (2a) and square planar Mn" (2b) sites within the *A*-site Mn column. The refined occupancies suggest a preference of Fe at the square planar (20.4%) over the tetrahedral environment of *A'* (8.0%). The same site preference was observed for Co and Ni in the $CaMnBReO_6$ (*B* = Co, Ni) analogs.[8] However Cr shows no preference with almost 20% substitution at both Mn sites. 5% *B*/Sb antisite disorder is observed for *B* = Cr, but *B* = Fe is more disordered with 13% inversion. Overall refined compositions are $CaMn_{0.81}Cr_{1.19}SbO_6$ and $CaMn_{0.85}Fe_{1.15}SbO_6$, showing that both materials are slightly Mn deficient. Secondary phase $MnCr_2O_4$ spinel[21] (0.2%) is observed in the *B* = Cr fit (Fig. 1).

Formal cation charges estimated using Bond Valence Sums (BVS's) from bond distances as shown in Table I are consistent with the nominal distribution $Ca^{2+}Mn^{2+}B^{3+}Sb^{5+}O_6$. Deviations such as apparent underbonding of the Mn sites reflect the cation disorder and strained nature of these quenched high pressure materials. The tendency for d^{10} Sb^{5+} to displace off-center is evidenced by a relatively high octahedral distortion factor Δ in the *B* = Cr structure, whereas the greater level of antisite disorder for *B* = Fe leads to a very regular average Sb/FeO_6 octahedron with small Δ. Ca sits in the large cuboctahedral void with a 10-fold coordination and all Ca-O distances between 2.36 and 2.80 Å, in good agreement with the typical bond lengths for Ca in other double double perovskites. [7,8,13]

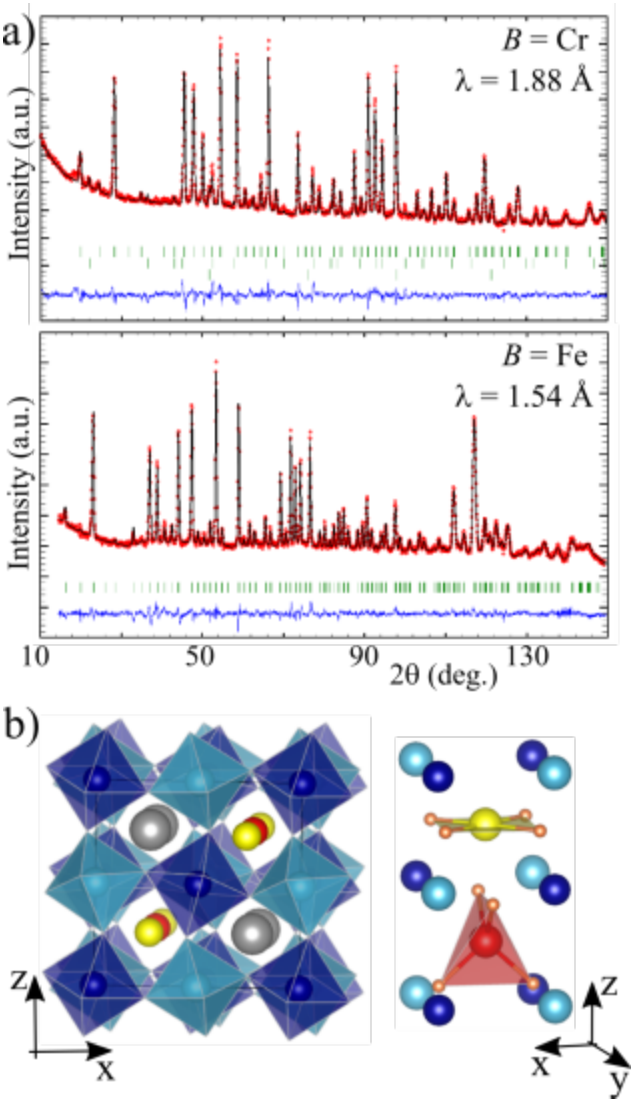

Fig.1. a) Rietveld fits of the double double perovskite $CaMnBSbO_6$ structures against 300 K NPD data. Top, *B* = Cr, secondary phase markers are for $MnCr_2O_4$ and V (sample holder); bottom, *B* = Fe. b) $P4_2/n$ $CaMnBSbO_6$ double double perovskite structure, with a view of the Mn'/Mn" *A*-site column to the right (*A*-cation Ca/Mn'/Mn" = grey/red/yellow; BO_6/SbO_6 octahedra = blue/cyan).

Octahedral tilt angles calculated from the *B*-O-Sb bond angles, are ϕ = 14.8(1)/17.1(1)° from the *z* axis and θ = 16.5(1)/16.6(1)° within the *xy* plane for *B* = Cr/Fe. These values lie within the range from 15 to

20º observed in the Mn*R*MnSbO$_6$ double double perovskite series.[5] These substantial tilts stabilise the columnar order of isovalent Ca and Mn cations within the *A* sites of the double double structure.

Table I. Atomic coordinates and interatomic distances (*d* in Å) for CaMn*B*SbO$_6$ from the Rietveld fits of 300 K NPD data using tetragonal space group *P4$_2$/n*. Lattice parameters *a* = 7.6320(2)/7.6616(1) Å and *c* = 7.6208(4)/7.6443(3) Å. Fitting reliability factors: R_p = 2.11/1.69%, R_{wp} =3.02/2.23%, R_f =5.44/3.51%, R_B = 7.80/5.60%, χ^2 = 7.17/3.32. Upper/lower or left/right values correspond to *B* = Cr/Fe.

Site (Wyckoff)	*x*	*y*	*z*	occ	B_{iso} (Å^2)	BVS[a]
Mn'/*B* (2a)	0.75	0.75	0.75	0.81/0.19(1) 0.912/0.088(3)	1.6(3) 0.01(1)	1.82 1.59
Mn"/*B* (2b)	0.25	0.25	0.75	0.82/0.18(1) 0.784/0.216(4)	1.6 0.01	1.33 1.27
Ca (4e)	0.25	0.75	0.7799(9) 0.7786(8)	1.0	2.8(1) 0.7(1)	2.08 2.05
B/Sb (4c)	0	0.5	0.5	0.952/0.048(5) 0.87/0.13(1)	0.64(8) 0.01	2.78 2.49
Sb/*B* (4d)	0	0	0.5	0.952/0.048(5) 0.87/0.13(1)	0.64 0.01	5.79 4.92
O1 (8g)	-0.041(1) -0.053(2)	0.552(1) 0.555(1)	0.2396(9) 0.244(1)	1.0	1.26(4) 0.14(2)	
O2 (8g)	-0.252(2) -0.244(2)	-0.0502(6) -0.0478(5)	0.5643(5) 0.5653(4)	1.0	1.26 0.14	
O3 (8g)	-0.252(2) -0.252(2)	0.0573(6) 0.0586(4)	-0.0345(7) -0.0345(4)	1.0	1.26 0.14	

d_{B-O1} (x 2)	2.048(8)/2.04(1)	d_{Sb-O1} (x 2)	1.895(8)/1.96(1)	d_{Ca-O1} (x 2)	2.70(1) / 2.77(1)
d_{B-O2} (x 2)	1.99(1) / 2.06(1)	d_{Sb-O2} (x 2)	2.02(1) / 1.97(1)	d_{Ca-O1} (x 2)	2.80(1) / 2.79(1)
d_{B-O3} (x 2)	1.99(1) / 2.00(1)	d_{Sb-O3} (x 2)	1.96(1) / 1.97(1)	d_{Ca-O2} (x 2)	2.590(7)/2.575(5)
$<d_{B-O}>$	2.01(1) / 2.03(1)	$<d_{Sb-O}>$	1.96(1) / 1.97(1)	d_{Ca-O3} (x 2)	2.45(1) / 2.445(7)
Δ[b][BO_6] x 10^4	1.85 / 1.53	$\Delta[SbO_6]$ x 10^4	6.79/ 0.08	d_{Ca-O3} (x 2)	2.36(1) / 2.373(7)
$d_{Mn'-O}$ (x 4)	2.080(5)/2.097(4)	$d_{Mn''-O}$ (x 4)	2.20(1) / 2.13(1)	$<d_{Ca-O}>$	2.58(1) / 2.59(1)

[a] BVS values estimated from interatomic distances as $V_i = \Sigma_j S_{ij} i = \exp(r_0 - r_{ij}/0.37)$, using R_0 values 1.79, 1.967, 1.724, 1.734 and 1.942 for Mn^{2+}, Ca^{2+}, Cr^{3+}, Fe^{3+} and Sb^{5+} respectively.[22]

[b] Δ is the octahedral distortion calculated from bond lengths as $\Delta = 1/6 * \Sigma [(d_i - d_{Av})/d_{Av}]^2$

Table II. Irreducible representations (Γ) and basis vectors (BV) from magnetic symmetry analysis of the *P4$_2$/n* CaMn*B*SbO$_6$ double double perovskites for propagation vector *k* = [0 0 0]. Moment coefficients m_x, m_y, m_z are shown for the *A*-site Mn and *B*-site BV's.

Symmetry operation	Γ_1		Γ_2		Γ_3	Γ_5	Γ_6
	BV_A	BV_B	BV_B	BV_A	BV_B	BV_A	BV_A
x,y,z	0 0 +	+ + +	+ + +	+ + 0	+ + + 0 0 0	0 0 +	+ + 0
–*x*+1/2, -*y*+1/2, *z*		− − +	− − +		+ + − 0 0 0		
–*y*, *x*+1/2, *z*+1/2	0 0 +	− + +	+ − −	+ + 0	0 0 0 − + +	0 0 −	− − 0
y+1/2, –*x*, *z*+1/2		+ − +	− + −		0 0 0 − + −		

B. Magnetic properties

Magnetic susceptibility measurements for CaMn*B*SbO$_6$ (*B* = Cr, Fe) samples are shown in Fig. 2. Curie-Weiss fits to the paramagnetic regions give paramagnetic moments of 7.45 and 7.59 μ_B for Cr and Fe samples respectively. Predicted spin-only moments are 7.07 and 8.36 μ_B; the poor agreement for *B* = Fe reflects the observed non-linearity of inverse susceptibility in the paramagnetic regime, which may result from the presence of magnetic impurities. Fitted Weiss contants of θ = -120 and -36 K for *B* = Cr and Fe show that dominant couplings between Mn and *B* spin sublattices are antiferromagnetic, as expected from GKA rules for their superexchange interactions, [23] and in keeping with their low temperature ferrimagnetic orders described below. The susceptibility data show a single ferrimagnetic Curie transition for CaMnCrSbO$_6$ at T_C = 49 K, but two magnetic transitions are observed for CaMnFeSbO$_6$, at T_{C1} = 55 and T_{C2} = 21 K.

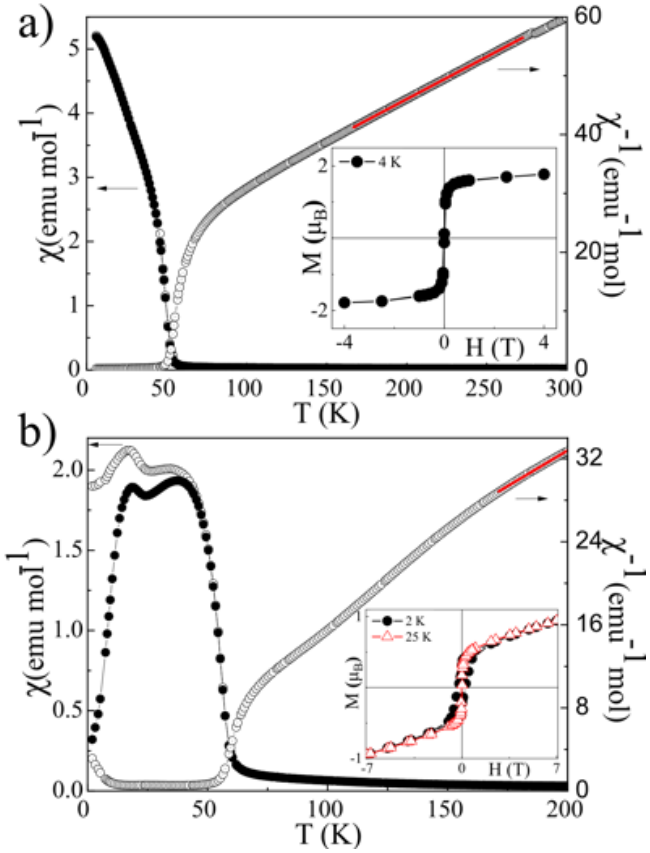

Fig 2. Magnetic susceptibility and hysteresis loops (insets) for CaMn*B*SbO$_6$; (a) *B* = Cr and (b) *B* = Fe. Curie-Weiss fits to inverse susceptibilities are also shown.

The magnetization-field loop for CaMnCrSbO$_6$ at 2 K shows a magnetization of 1.55 μ_B at zero field increasing to 1.77 μ_B at 4 T, consistent with the expected value of 2 μ_B for ferrimagnetic order of antiparallel Mn^{2+} $S = 5/2$ and Cr^{3+} $S = 3/2$ spins. Loops for the Fe analog at 2 and 25 K are very similar showing that the type of magnetic order does not change at T_{C2} = 21 K. The coercive field of 0.2 T at 2 K shows that CaMnFeSbO$_6$ has appreciable magnetic anisotropy. An ideal ferrimagnetic order of Mn^{2+} and Fe^{3+} $S = 5/2$ spins would lead to zero net moment. The small 0.4 μ_B observed moment, increasing to 0.94 μ_B at 7 T likely reflects cation disorder, in particular the 13% Fe/Sb cation inversion at the *B*-sites.

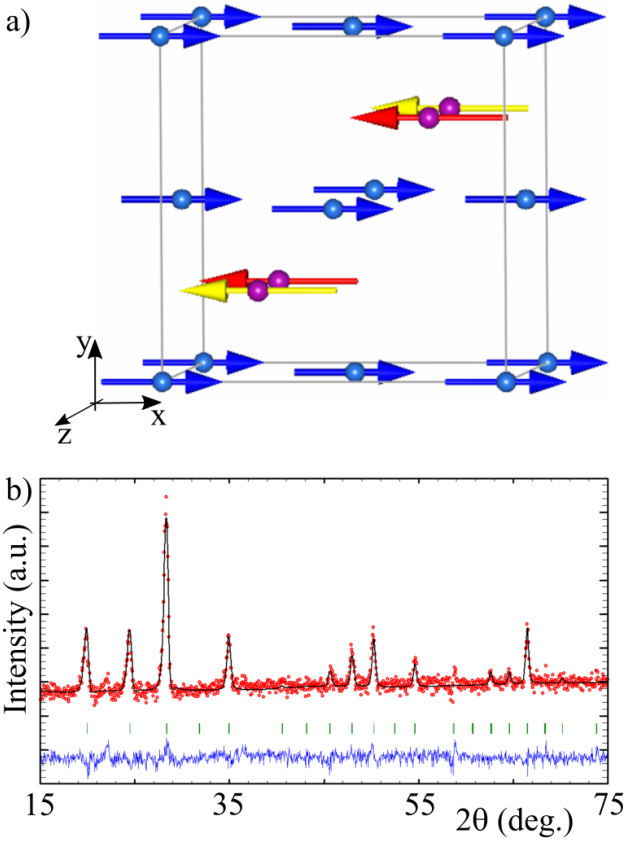

Fig 3. Magnetic structure determination for CaMnCrSbO$_6$. (a) Spin structure where red/yellow/blue arrows represent, Mn'/Mn"/*B* = Cr site spins. (b) Rietveld fit to the 1.5 – 65 K NPD difference pattern. The first three magnetic peaks (observed in the range 2θ = 15 to 30°) are (110)/(101), (111), and (200)/(002).

NPD patterns recorded below the Curie transitions reveal magnetic diffraction peaks that index with propagation vector *k* = [0 0 0], and the resulting magnetic symmetry analysis for the CaMn*B*SbO$_6$ phases is summarized in Table II. The magnetic intensities in the 1.5 – 65 K NPD difference pattern for CaMnCrSbO$_6$ are fitted by irreducible representation (Irep) Γ_3 with moments in the *xy* plane. The refined magnetic moments of 3.72(3) and 2.82(3)

μ_B respectively at Mn^{2+} (with tetrahedral and square-planar site values constrained to be equal) and Cr^{3+} sites are reduced from ideal spin-only values of 5 and 3 μ_B due to cation disorder and frustration. This model corresponds to the simple ferrimagnetic arrangement expected from the magnetization data, and is shown in Fig. 3a with the final fit to the magnetic diffraction intensities in Fig. 3b.

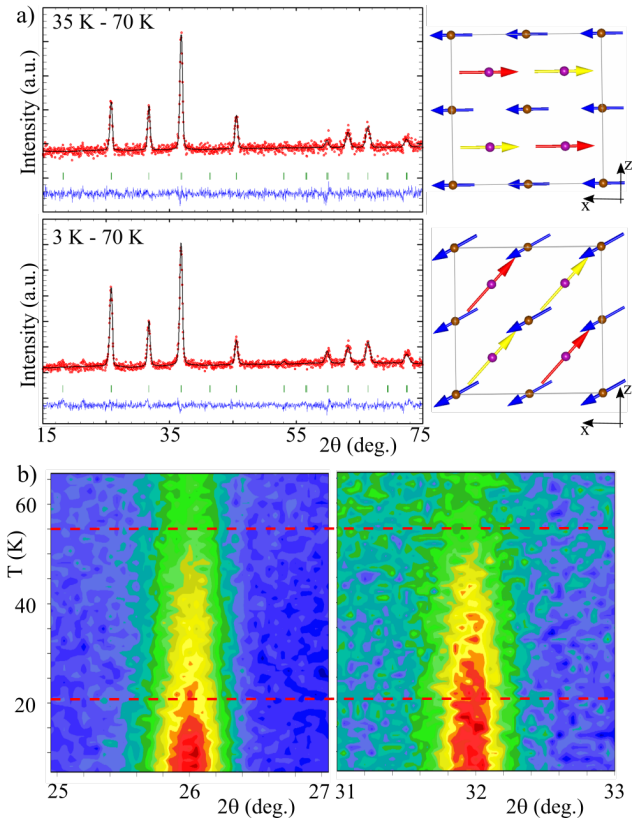

Fig. 4. a) Rietveld fits to the $CaMnFeSbO_6$ NPD difference patterns 35-70 K and 3–70K. The first three prominent magnetic peaks (observed in the range 2θ = 25 to 40°) are (110)/(101), (111), and (200)/(002). The right panels show the refined magnetic structures at 35 (top) and 3 K (bottom). b) 2D NPD short scan data showing the different thermal evolution of (110) and (111) magnetic peaks (left and right respectively). T_{C1} and T_{C2} are labeled as red dashed lines.

At 35 K, below the first magnetic transition at T_{C1} = 55 K, $CaMnFeSbO_6$ shows the same spin arrangement as for $CaMnCrSbO_6$, with magnetic moments of 3.00(4) and 2.17(3) μ_B for Mn^{2+} and Fe^{3+} respectively. Changes to the magnetic diffraction intensities are observed on cooling through the second transition (T_{C2} = 21 K) to 3 K, as shown in Fig. 4. Fits to the 3 – 70 K NPD magnetic intensities reveal that additional spin components parallel to the z axis that follow the Γ_1 Irep are present. The T_{C2} transition thus corresponds to a spin reorientation out of the xy plane, as shown in Fig. 4a. The total refined magnetic moments of 3.89(6) and 2.78(15) μ_B for Mn^{2+} and Fe^{3+} respectively at 3 K (Table III), show that the Fe value is somewhat reduced from the ideal value of 5 μ_B, again reflecting the Fe/Sb antisite disorder.

Fits to the short neutron scans for $CaMnFeSbO_6$ were used to extract the temperature dependences of the magnetic moments as shown in Fig. 5. Critical fits shown on Fig. 5a confirm that the μ_z components disorder at T_{C2} = 22(1) K for exponent β = 0.35(2) while μ_z components decrease to zero at T_{C1} = 52.1(3) K for β = 0.4(1). The critical exponents are in agreement with the theoretical value of β = 0.365 for a 3D-Heisenberg magnet.

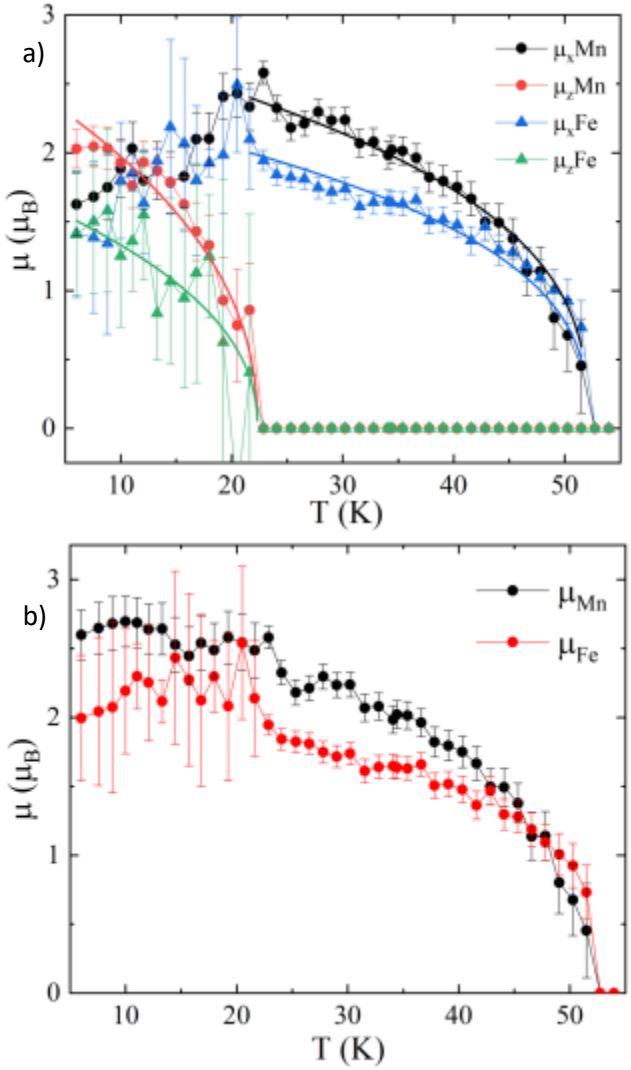

Fig. 5. Temperature variations of a) the μ_x and μ_z components, and b) the resultant moments μ, at Mn and Fe sites from Rietveld fits to the short NPD scans for $CaMnFeSbO_6$. Critical fits shown to the μ_x and μ_z components are described in the text.

The spin reorientation transition at T_{C2} = 21 K is likely driven by magnetic anisotropy effects which are evidenced by the moderate coercivity of 0.2 T at 2 K in magnetization data (Fig. 2b). The tilt of the Fe spin directions out of the *xy*-plane (33º at 3 K) observed by NPD is of comparable magnitude to the FeO_6 octahedral tilting angle of ϕ = 17º measured in the crystal structure analysis. However, the octahedral tilts from the *c*-axis are out-of-phase (Fig. 1b; the overall tilt scheme is $a^+a^+c^-$ in Glazer notation[5]) with half of the octahedra tilted by $+\phi$ and the other half by $-\phi$. All Fe moments are parallel so only half are tilted in the same direction as their FeO_6 octahedra, hence there is an equivalent anisotropy-stabilised magnetic ground state in which μ_z components are reversed relative to the directions shown in Fig. 4a (lower right). Thermal fluctuations between these two states on warming likely lead to the spin reorientation transition at T_{C2} = 21 K above which μ_z components become dynamic with static components only present in the *xy* plane up to T_{C1} = 55 K.

Table III. Refined components of the magnetic moments in the *xy* plane (shown as μ_x as spin directions within the *xy* plane are not determined) and parallel to the *z*-axis (μ_z) axis for CaMn*B*SbO_6 at low temperatures.

B	*T* (K)	Site	μ_x (μ_B)	μ_z (μ_B)	μ_{tot} (μ_B)
Cr	1.5	Mn	3.72(3)	0	3.72(3)
		B	2.82(3)	0	2.82(3)
Fe	35	Mn	3.00(4)	0	3.00(4)
		B	2.17(3)	0	2.17(3)
Fe	3	Mn	2.62(8)	2.87(5)	3.89(6)
		B	2.34(11)	1.51(16)	2.78(15)

Although second magnetic transitions below T_C have been observed in other double double perovskites, these have been due to low tempeature orders of other spin sublattices; of Nd^{3+} moments in $MnNdMnSbO_6$;[5] and of Mn spins in CaMn*B*ReO_6 (*B* = Mn, Fe).[7] In $CaMnFeSbO_6$, both Mn^{2+} and Fe^{3+} spins order at T_{C1} = 55 and reorient below T_{C2} = 21 K. It is surprising that the Fe phase shows a spin reorientation transition whereas the Cr analog does not, as both *B* = Cr^{3+} and Fe^{3+} cations have non-degenerate ground states. This is not likely to be due to structural effects of differing degrees of *B*/Sb antisite cation disorder, as *B* = Cr has less (5%) disorder than *B* = Fe (13%), and greater disorder would be more likely to suppress a coherent rotation of spin directions. The spin rotation may reflect the greater magnetic disorder for *B* = Fe due to the larger *B*/Sb antisite disorder, as the saturated low-temperature *B*-site moment of 2.8 μ_B is substantially below the ideal value of 5 μ_B for Fe^{3+}, whereas the 2.8 μ_B value for *B* = Cr is close to the ideal 3 μ_B Cr^{3+} moment. Charge transfer between *A*-site Mn^{2+}/Fe^{2+} and B^{3+} cations for *B* = Fe, but which is unlikely for *B* = Cr, may also generate small differences in anisotropy between *B* = Cr and Fe structures that are sufficient to stabilise the tilted spin ground state only in the latter material. X-ray absoption spectroscopy study of the transition metal valence states would be useful to give further insight into the different magnetic properties of these two new double double perovskites.

IV. CONCLUSIONS

The two new double double perovskites CaMn*B*SbO_6 (*B* = Cr, Fe) oxides can be recovered from high pressure and high temperature conditions. Both have tetragonal $P4_2/n$ crystal structures with cation disorder that leads to slight Mn-deficiency with neutron-refined compositions $CaMn_{0.81}Cr_{1.19}SbO_6$ and $CaMn_{0.85}Fe_{1.15}SbO_6$. Both materials have collinear ferrimagnetic *xy*-plane spin orders with *A*-site Mn moments antiparallel to those at the *B* sites below 49 and 55 K for *B* = Cr and Fe respectively. However, *B* = Fe shows a second transition at 21 K where spins reorient towards the *z* axis. It is not clear why a reorientation transition is not also observed for *B* = Cr, but a greater degree of magnetic disorder for *B* = Fe and possible *A*-*B* intersite charge transfer may be significant.

ACKNOWLEDGEMENTS

The authors thank EPSRC for funding and STFC for provision of beamtime at ILL. K.N.A. acknowledges funding from King Abdulaziz City for Science and Technology (KACST).

References

[1] S. Vasala and M. Karppinen. Prog. Solid State Chem., **43**, 1-36 (2015).
[2] G. King, and P. M. Woodward. J. Mater. Chem. **20**, 5785 (2010).
[3] G. King, S. Thimmaiah, A. Dwivedi and P. M. Woodward. Chem. Mater. **19**, 6451 (2007).
[4] M.C. Knapp and P.M. Woodward. J. Solid State Chem. **179**, 1076 (2006).
[5] E. Solana-Madruga, Á. M. Arévalo-López, A. J. Dos Santos-García, E. Urones-Garrote, D. Ávila-Brande, R.

Sáez-Puche, and J. P. Attfield, Angew. Chem. Int. Ed. **55**, 9340 (2016).
[6] E. Solana-Madruga, Á. M. Arévalo-López, A. J. Dos santos-García, C. Ritter, C. Cascales, R. Sáez-Puche and J. P. Attfield. *Phys. Rev. B* **97**, 134408 (2018).
[7] G. M. McNally, Á. M. Arévalo-López, P. Kearins, F. Orlandi, P. Manuel and J. P. Attfield. C*hem. Mater.* **29**, 20, 8870–8874 (2017).
[8] E. Solana-Madruga, Y. Sun, A. M. Arévalo-López and J. P. Attfield. *Chem. Comm.* **55**, 2605 (2019).
[9] J. M. De Teresa, D. Serrate, J. Blasco, M. R. Ibarra, and L. Morellon, *Phys. Rev. B* **69**, 144401 (2004).
[10] M. Sikora, O. Mathon, P. van der Linden, J. M. Michalik, J. M. de Teresa, Cz. Kapusta, and S. Pascarelli, *Phys. Rev. B* **79**, 220402(R) (2009).
[11] M. R. Li, M. Retuerto, Z. Deng, P. W. Stephens, M. Croft, Q. Huang, H. Wu, X. Deng, G. Kotliar, J. Sánchez-Benítez, J. Hadermann, D. Walker, and M. Greenblatt, *Angew. Chem., Int. Ed.* **54**, 12069 (2015).
[12] A. M. Arévalo-López, G. M. McNally, and J. P. Attfield, *Angew. Chem., Int. Ed.* **54**, 12074 (2015).
[13] G. M. McNally, A. M. Arévalo-López, F. Guillou, P. Manuel and J. P. Attfield. *Phys. Rev. Mat.* **4**, 064408 (2020).
[14] M. Retuerto, J.A. Alonso, M. Garcia-Hernandez and M.J. Martinez-Lope. Solid State Commun. **139**, 19–22 (2006).
[15] P. D. Battle, T. C. Gibb, A. J. Herod, S.-H. Kim and P. H. Munns, *J. Mater. Chem.*, **5**, 865 (1995).
[16] A. J. Dos santos-García, E. Solana-Madruga, C. Ritter, D. Ávila-Brande, O.Fabelo and R. Sáez-Puche. *Dalton Trans.*, **44**, 10665-10672 (2015).
[17] A. J. Dos santos-García, C. Ritter, E. Solana-Madruga, R. Sáez-Puche. *J. Phys.: Condens. Matter.*, **25**, 206004 (2013).
[18] J. Rodríguez-Carvajal. BasIreps: A program for calculating irreducible representation of little groups and basis functions of polar and axial vector properties. User Manual, 2004.
[19] J. Rodriguez-Carvajal, Physica B, **192**, 55 (1993).
[20] R. D. Shannon and C. T. Prewitt, *Acta Cryst. B*, **25**, 925–946 (1969).
[21] N. Mufti, G.R. Blake and T.T.M. Palstra. *J. Magn. Magn. Mater.* **321**, 1767–1769 (2009).
[22] I. D. Brown, The Chemical Bond in Inorganic Chemistry: The Bond Valence Model, Oxford University Press, 2002.
[23] J. B. Goodenough. Magnetism and the Chemical Bond, New York: Wiley, 1963.